Activation of Apical Chloride Channels in the Gastric Oxyntic Cell

JEFFERY R. DEMAREST,* DONALD D. F. LOO,† GEORGE SACHS

Oxyntic cells that retain distinct morphological polarity between apical and basolateral membranes were isolated from the gastric mucosa of the amphibian *Necturus*. Patch-clamp techniques were applied to these cells to identify apical membrane ion channels associated with hydrochloric acid secretion. A single class of voltage-dependent, inwardly rectifying chloride channels was observed in the apical membranes of both resting and stimulated (acid-secreting) oxyntic cells. Stimulation of the cells with dibutyryladenosine 3′,5′-monophosphate and isobutylmethylxanthine increased channel open probability and simultaneously increased apical membrane surface area. This chloride channel is probably responsible for electrogenic chloride secretion by the gastric mucosa and may also participate in the fluid- and enzyme-secretory functions of the oxyntic cell, analogous to the chloride channels found in the apical membranes of other exocrine cells.

IN RESPONSE TO THE HORMONES HISTAMINE, acetylcholine, and gastrin, oxyntic cells of the gastric mucosa secrete a solution of hydrochloric acid that has a *p*H of about 0.8 and is isotonic to plasma. Secretion is initiated by the fusion of intracellular membrane vesicles with the apical (secretory) membrane, resulting in up to a 40-fold expansion of the apical membrane area in mammals (*1*). These vesicles contain H^+- and K^+-dependent adenosine 5′-triphosphatase (H^+,K^+-ATPase), the H^+ pump that exchanges luminal K^+ for cytosolic H^+ (*2*). Concurrently activated Cl^- and K^+ transport pathways in the apical membrane supply Cl^- to accompany the actively transported H^+ and K^+ to replenish luminal K^+ depleted by the ATPase. Although acid secretion characterizes the oxyntic cell, the activation of apical Cl^- permeability pathways is a common phenomenon during the stimulation of most exocrine cells.

Ion permeability pathways in the apical membrane of oxyntic cells from the rabbit mucosa have been studied in isolated membrane vesicles and digitonin-permeabilized gastric glands. Initial studies of vesicles from stimulated mucosa indicated that K^+ and Cl^- were cotransported (*3*). However, later investigations found that there was a Cl^- conductance alone (*4*) or that Cl^- and K^+ conductances were present in parallel (*5*). Studies of the acid-transporting compartment in permeabilized rabbit gastric glands were consistent with the presence of a Cl^- conductance but not of a K^+ conductance (*6*). Vibrating probe studies of *Necturus* gastric mucosa have shown that oxyntic cells alone are responsible for electrogenic Cl^- secretion (*7*).

We have found that *Necturus* oxyntic cells isolated by enzymatic digestion in the presence of the histamine type-2 receptor blocker cimetidine retain distinct apical to basolateral membrane polarity (*8*). Stimulation of these cells results in an increase in apical membrane area similar to that observed in the intact mucosa. Access to the exposed apical membrane has enabled us to apply single-channel recording techniques to investigate the presence of Cl^- channels (*9*, *10*).

Light microscopy of the isolated oxyntic cells revealed clusters of cells surrounding the lumen of a partially dispersed gastric gland (Fig. 1A). These cells showed distinct membrane polarity similar to that found in oxyntic cells in situ (*1*), with a granular-appearing apical membrane bordering the lumen and with the basolateral membrane distant from the lumen being marked by a relatively smooth surface. Concurrent stimulation of the cells with dibutyryladenosine 3′,5′-monophosphate (dibutyryl cAMP) (*11*) and the phosphodiesterase inhibitor isobutylmethylxanthine (IBMX) increased the apical membrane area (Fig. 1B). The time course of this morphological change in the isolated cells was similar to that observed by microscopy in the intact, isolated amphibian mucosa (*1*) and is also consistent with that for the stimulation-induced increase in capacitance measured in the intact mucosa by impedance analysis (*12*).

Recordings of currents were obtained for a cell-attached patch on the apical membrane of a resting cell (Fig. 1C, left). The pipette potential (V_p) of 20 mV with reference to the bathing solution corresponds to hyperpolarization of the resting membrane potential. Downward deflections of the current trace indicate either the entry of cations from the pipette into the cell or anion exit from the cell into the pipette. Stimulation of the resting oxyntic cell with dibutyryl cAMP and IBMX progressively increased channel activity within 10 to 15 min, with activity reaching a plateau at 20 to 30 min (Fig. 1C,

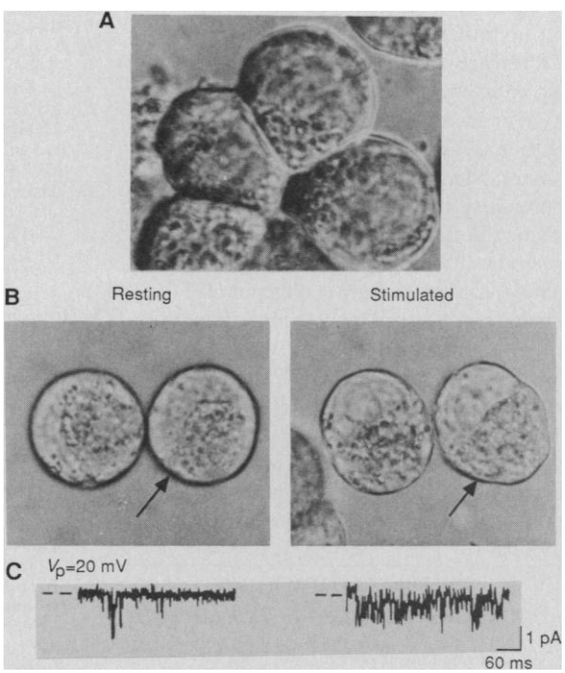

Fig. 1. Morphology of isolated oxyntic cells (A and B) and the activation of apical ion channels (C). (**A**) Bright-field photomicrograph (×400) of resting cells showing a partially dispersed gastric gland composed of a rosette of cells surrounding a lumen. (**B**) Two isolated resting oxyntic cells (left); the same cells (right) after 30 min of stimulation with 1 m*M* dibutyryl cAMP and 0.1 m*M* IBMX. In both panels, the granular-appearing apical membrane is indicated by the arrows. (**C**) The left panel shows a single-channel current record (filtered at 3 kHz) for a cell-attached patch (at V_p = 20 mV) on the apical membrane of a resting cell. The dashed line indicates baseline. The right panel shows a current record for the same cell after 20 min of stimulation with 1 m*M* dibutyryl cAMP and 0.1 m*M* IBMX. The pipette contained 110 m*M* KCl, 1 m*M* NaCl, 1 m*M* $MgCl_2$, 6.01 m*M* $CaCl_2$, 10 m*M* EGTA, and 10 m*M* Hepes-KOH (*p*H 7.3). The Ca^{2+} concentration was calculated to be 100 n*M* (*9*). The bath solution was NaCl Ringer. Experiments were performed at 20° to 23°C.

J. R. Demarest and G. Sachs, Center for Ulcer Research and Education, Wadsworth Veterans Administration Medical Center, Los Angeles, CA 90073.
D. D. F. Loo, Department of Physiology, UCLA School of Medicine, Center for the Health Sciences, Los Angeles, CA 90024.

*Present address: Department of Zoology, 632 Science-Engineering, University of Arkansas, Fayetteville, AR 72701.
†To whom correspondence should be addressed.

right). The open probability (P_o) of the channel, estimated as the ratio of the sum of the durations of all the individual channel openings to the total time analyzed, for cell-attached patches held at a V_p of 20 mV increased from $(0.2 \pm 0.1) \times 10^{-2}$ (mean ± SEM) in resting cells to $(5.8 \pm 2.4) \times 10^{-2}$ ($n = 4$; $P < 0.001$) after stimulation. The channel conductance at a V_p between 20 and 50 mV was 13 ± 2 pS ($n = 4$). The time course of the increase in dibutyryl cAMP–stimulated channel activity as indicated by P_o was similar to that of the onset of acid secretion in the intact mucosa after stimulation (*13*).

In 40 cell-attached patches formed on the apical membranes of resting cells, which were subsequently stimulated with dibutyryl cAMP and IBMX, this type of channel was the only one observed. Approximately 50% of the cell-attached patches on the apical membrane of resting cells showed channel activity, and 76% of the resting patches without channel activity showed activation of a channel after stimulation. In total, 88% of the patches with acceptable seal resistances (>7 gigaohms) had channels, either before or after stimulation.

In cell-attached patches inward currents were observed at hyperpolarizing potentials (Fig. 2A), and current became outward at large depolarizing potentials ($V_p = -100$ mV). An increase in P_o was observed with increasing hyperpolarization; P_o increased by almost two orders of magnitude as V_p was increased from 20 to 50 mV.

The current-voltage relation (*I-V*) for the channel was determined (Fig. 2B). We obtained the membrane potential shown on the abscissa by assuming a resting potential of −50 mV, a value we determined with intracellular microelectrodes and a value that is similar to those obtained previously (*8*). Currents through the channel rectified inward. Single-channel conductance was 10 pS at depolarizing potentials between 20 and 50 mV and increased to 46 pS at extreme hyperpolarizing potentials between −150 and −100 mV. Stimulation of acid secretion in the isolated intact epithelium results in a hyperpolarization of the apical membrane of the oxyntic cells (*13*). Such a hyperpolarization would increase the conductance and P_o of these channels, both of which would contribute to the increase in macroscopic conductance of the apical membrane (*13*). The reversal potential for the channel is −20 mV, different from the value of −40 mV observed for K^+ channels found in the basolateral membranes of these cells (*9*) but close to that expected for a Cl^- channel in a Cl^- secretory cell with a relatively high intracellular Cl^- activity (*14*).

A current record was obtained for a cell-attached patch on a stimulated oxyntic cell with the pipette containing the presumably impermeant ions *N*-methyl-D-glucamine gluconate (NMDG glu) (Fig. 2C). At a V_p of 20 mV, inward currents were again observed. This activity is only consistent with anions exiting from the cell. Similar results were observed when only K^+ in the pipette solution was replaced with $NMDG^+$.

We also examined the effect of Ba^{2+}, a K^+-channel blocker, on excised inside-out patches. For a particular patch containing a single 19-pS channel and held at a V_p of 20 mV before and after the addition of 1 m*M* Ba^{2+} to the bath solution, the size of the current steps (0.85 ± 0.01 pA), the mean open time (1.5 ± 0.1 ms), and the mean closed time (56.4 ± 13.6 ms) were all unaffected by Ba^{2+}. The P_o was slightly increased in the presence of Ba^{2+} from 1.69×10^{-2} to 2.42×10^{-2}. Similar data were obtained for two additional experiments. Thus, the channel did not exhibit any of the effects expected for Ba^{2+} block of a K^+ channel.

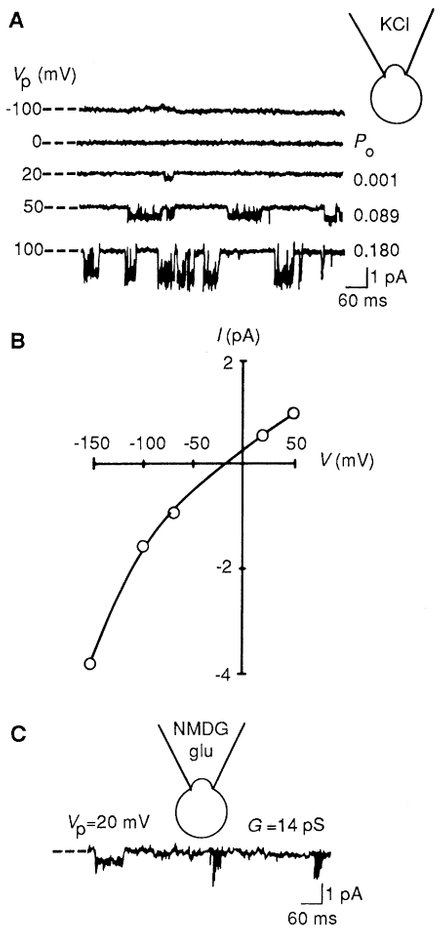

Fig. 2. (**A**) Single-channel current records (filtered at 3 kHz) for a channel in a cell-attached patch on the apical membrane. The pipette and bath solutions were as in Fig. 1C. The dashed line indicates baseline. (**B**) The *I-V* relation of the channel shown in (A). Membrane potential, shown on the abscissa, assumes an intracellular potential of −50 mV (see text). An additional point corresponding to a V_p of 70 mV, not shown in (A), is included. (**C**) Current records (filtered at 500 Hz) of a cell-attached patch (at V_p = 20 mV) formed on a stimulated cell with a pipette containing NMDG glu. Single-channel conductance (*G*) was 14 pS.

Our results indicate that the channels in the apical membranes of oxyntic cells are Cl^- channels. The characteristics of these channels would favor the efflux of Cl^- from the cytosol, and their activity is modulated by voltage and cAMP. Apart from their probable function in acid secretion, these channels may also be responsible for electrogenic Cl^- secretion and may play a role in fluid and pepsinogen secretion from oxyntic cells (*7*, *15*).

We found no evidence for an apical K^+ channel in oxyntic cells. Such an absence of K^+ channels is consistent with the observations that increasing mucosal K^+ concentration or addition of 20 m*M* Ba^{2+} to the mucosal solution did not affect Cl^- and H^+ secretion in the intact epithelium (*16*). The currently accepted model of HCl secretion across the apical membranes of oxyntic cells invokes both Cl^- and K^+ conductances in parallel with an active electroneutral exchange of H^+ for K^+ by the H^+,K^+-ATPase (*5*). Our data are inconsistent with this model, supporting instead a Cl^- conductive channel alone. The absence of evidence for an apical K^+ channel suggests that K^+ exits the cell via a nonchannel mechanism.

Our study also shows that the oxyntic cell is a useful model for studying stimulus-secretion coupling and membrane fusion. Because of the segregation of channel types, the oxyntic cell could also have potential uses for studies on protein sorting, lateral membrane diffusion, and maintenance of epithelial cell polarity.

REFERENCES AND NOTES

1. H. F. Helander and B. I. Hirschowitz, *Gastroenterology* **63**, 951 (1972); T. M. Forte, T. E. Machen, J. G. Forte, *ibid.* **73**, 941 (1977); C. D. Logsdon and T. E. Machen, *Anat. Rec.* **202**, 73 (1982).
2. A. L. Ganser and J. G. Forte, *Biochim. Biophys. Acta* **307**, 169 (1973); G. Sachs *et al.*, *J. Biol. Chem.* **251**, 7690 (1976).
3. J. M. Wolosin and J. G. Forte, *J. Membr. Biol.* **71**, 195 (1983).
4. J. Cuppoletti and G. Sachs, *J. Biol. Chem.* **259**, 14952 (1984).
5. J. M. Wolosin and J. G. Forte, *Am. J. Physiol.* **246**, C537 (1984).
6. A. Perez, D. Blissard, G. Sachs, S. J. Hersey, *ibid.* **256**, G305 (1989).
7. J. R. Demarest, C. Scheffey, T. E. Machen, *ibid.* **251**, C643 (1986).
8. The gastric mucosa is a simple epithelium containing infoldings, the gastric glands, which contain parietal and chief cells in mammals and oxyntic cells in amphibia. The latter contain both the acid- and zymogen-secretory systems. We have used oxyntic cells from *Necturus* because of their large size and have modified a previously described isolation meth-

od [A. L. Blum *et al.*, *Gastroenterology* **61**, 189 (1971)]. The underlying muscle layer of the fundic mucosa was removed, and the tissue was incubated for 2 hours with Pronase, collagenase type IV, and bovine serum albumin, each at 1 mg/ml, and 0.1 m*M* cimetidine in a NaCl Ringer solution containing 85 m*M* NaCl, 4 m*M* KCl, 20 m*M* $NaHCO_3$, 1.0 m*M* $CaCl_2$, 1.0 m*M* $MgCl_2$, 1.0 m*M* KH_2PO_4, 5 m*M* glucose, and 10 m*M* Hepes that had been equilibrated with 95% O_2:5% CO_2 to *p*H 7.3. After incubation, the surface cells were removed by blotting the mucosal surface on absorbent paper. The tissue was subsequently shaken in a small volume of NaCl Ringer solution to release the oxyntic cells. The patch-clamp methods used have been described previously (*9*). Gigaohm seals were formed on the apical membranes of isolated oxyntic cells placed in a chamber on the stage of an inverted microscope.

9. S. Ueda, D. D. F. Loo, G. Sachs, *J. Membr. Biol.* **97**, 31 (1987).
10. We studied patches of the apical membrane because it was morphologically distinct (Fig. 1) and because the basolateral membrane of oxyntic cells does not contain a Cl^- conductance as determined from rapid solution-change experiments on cells impaled with microelectrodes across their basolateral membranes in the intact epithelium. Reducing basolateral Cl^- concentration to one-tenth of its normal concentration results in a slight hyperpolarization of the basolateral membrane potential and has no effect on the ratio of apical to basolateral membrane resistances (J. R. Demarest, unpublished data).
11. S. Nakajima, R. L. Shoemaker, B. I. Hirschowitz, G. Sachs, *Am. J. Physiol.* **219**, 1259 (1970).
12. C. Clausen, T. E. Machen, J. M. Diamond, *Science* **217**, 448 (1982).
13. J. R. Demarest and T. E. Machen, *Am. J. Physiol.* **249**, C535 (1985).
14. For example, the intracellular Cl^- activity measured in acinar cells of the rabbit submandibular gland with ion-selective microelectrodes is 42 to 44 m*M* [K. R. Lau and R. M. Case, *Pfluegers Arch.* **411**, 670 (1988)]. If we take −20 mV as the reversal (Nernst) potential for the channel shown in Fig. 2B, the intracellular Cl^- activity in the oxyntic cell would be 42.6 m*M*, assuming an activity coefficient of 0.76 for the Ringer solution and the cell interior.
15. O. H. Petersen, *Am. J. Physiol.* **251**, G1 (1986); R. C. De Lisle and U. Hopfer, *ibid.* **250**, G489 (1986).
16. M. Schwartz, A. D. Pacifico, T. N. Mackrell, A. Jacobson, W. S. Rehm, *Proc. Soc. Exp. Biol. Med.* **127**, 223 (1968); W. L. McLennan, T. E. Machen, T. Zeuthen, *Am. J. Physiol.* **239**, G151 (1980).
17. Supported by Smith Kline Beckman fellowships to D.D.F.L. and J.R.D., NIH grant DK38664 to J.R.D. and NIH grants AM17328 and DK40615 to G.S., and a U.S. Veterans Administration Senior Medical Investigator award to G.S.

13 January 1989; accepted 18 April 1989

The Location of DNA in RecA-DNA Helical Filaments

E. H. EGELMAN* AND X. YU*

The helical filament that the RecA protein of *Escherichia coli* forms around DNA is the active apparatus in protein-catalyzed homologous genetic recombination. The actual position of DNA within this complex has been unknown. Image analysis has been performed on electron micrographs of filaments of RecA on double-stranded DNA and on single-stranded DNA to visualize a difference that is consistent with one strand of the double-stranded DNA. This localization of the DNA gives additional information about the unusual structure of DNA in the complex with RecA protein.

THE RECA PROTEIN OF *Escherichia coli* has been the most extensively studied enzyme of general (homologous) genetic recombination (*1–3*). In in vitro systems this enzyme alone can mediate the recognition and strand exchange between two homologous DNA molecules, the central events in homologous recombination. The biologically active form of the RecA molecule, both in vivo (*4*) and in vitro (*5, 6*), is a polymer, and all available evidence suggests that the structural framework for the strand exchange is a helical polymer of RecA that forms around one DNA molecule that is either single-stranded or has a single-stranded region. Homologous recognition and strand exchange then occur when a homologous DNA molecule is brought into this complex. We report a direct localization of a significant feature that we interpret to be the DNA within the complex initially formed by RecA around a DNA molecule. This observation, based on conventional negative-stain electron microscopy, was made possible by image processing that has revealed a feature (one strand of DNA) that accounts for about 2.5% of the total mass of the complex. The method we have used is both simple and powerful and can readily be applied to other polymeric protein-DNA structures.

RecA filaments were prepared on both single-stranded DNA (ssDNA) and double-stranded DNA (dsDNA) in the presence of a relatively nonhydrolyzable adenosine triphosphate (ATP) analog, ATP-γ-S. Filaments were negatively stained with uranyl acetate, and electron micrographs were taken on film (Fig. 1). Images of more than 100 filament sections (where each filament section was typically from 1500 to 3000 Å long) were scanned with a digital densitometer, corrected for curvature (7), and Fourier-transformed. The Fourier transform of the projection of a helical object is nonzero everywhere except on layer lines, where the spacing of the layer lines is related to the pitch of the helices from which they arise (*8*). Three layer lines were extracted from each filament transform (Bessel function order 0, 1, and 2), all arising from the right-handed 95 Å pitch helix in the RecA filament. After filaments with marginal data were excluded, two average data sets were generated: a RecA-ssDNA set from 44 filaments and a RecA-dsDNA set from 39 filaments. The up-down phase residuals (*9*) for each of the individual filaments against the average, which is a measure of both the polarity of the structure and the quality of the data, are shown in Fig. 2. The averaged layer line data were then used to generate the helically projected density distribution of the filament (Fig. 3), which corresponds to a cross section of the filament that has been averaged along the 95 Å pitch helix.

Because the difference between the two data sets has a component that is due entirely to noise (sample statistics) and a component that is physically meaningful but small, we have generated a difference map that is expressed in units of standard errors. To do this, we have determined the standard error of the mean (SEM) at every pixel in each of the two average maps,

$$\mathrm{SEM}_{i,j} = \frac{\left[\sum_{k=1}^{n} (\rho_{i,j}{}^{k})^2 - \left(\sum_{k=1}^{n} \rho_{i,j}{}^{k}\right)^2\right]^{1/2}}{[(n-1)n]^{1/2}} \quad (1)$$

where $\rho_{i,j}{}^{k}$ is the density at point i,j in the kth map. The standard error at every point in the difference map is then:

$$\sigma_{i,j}{}^{\mathrm{dif}} = [(\mathrm{SEM}_{i,j}{}^{\mathrm{ds}})^2 + (\mathrm{SEM}_{i,j}{}^{\mathrm{ss}})^2]^{1/2} \quad (2)$$

The densities in the difference map can then be divided by the standard error at every point in the difference map to show the significance of features. The result is shown in Fig. 3, in which only one strong feature emerges, with a peak value of 4.8 standard errors. This feature is thus quite significant statistically, and we interpret it to be one strand of the dsDNA and not a conformational change of the protein or the staining pattern, for four reasons.

1) Because the DNA in the RecA-DNA complex follows the RecA helix, stereochemical constraints dictate that the axis of the dsDNA cannot be more than 17 Å radially from the RecA filament axis (*10*). The feature that we observed is centered at a radius of about 7 Å, consistent with this constraint.

2) The DNA within the RecA-DNA complex must be accessible to external DNA molecules. Parts of DNA in the complex with RecA can be methylated by dimethyl

Department of Molecular Biophysics and Biochemistry, Yale University, New Haven, CT 06511.

*Present address: Department of Cell Biology and Neuroanatomy, University of Minnesota, Minneapolis, MN 55455.